Ionization of many-electron atoms by the action of two plasma models

Michael-Adán Martínez-Sánchez, César Martínez-Flores ◉, Rubicelia Vargas, and Jorge Garza[*]

División de Ciencias Básicas e Ingeniería, Departamento de Química, Universidad Autónoma Metropolitana-Iztapalapa,
San Rafael Atlixco 186, Col. Vicentina, 09340 Iztapalapa, México City, México

Remigio Cabrera-Trujillo ◉

Instituto de Ciencias Físicas, Universidad Nacional Autónoma de México, Avenida Universidad S/N,
Cuernavaca, Morelos 62210, México

K. D. Sen ◉[†]

School of Chemistry, University of Hyderabad, Hyderabad 500 046, India

The Hartree-Fock equations for many-electron atoms embedded in a plasma medium are solved using two different plasma models: (a) Debye-Hückel screening (DHS) potential and (b) exponential cosine screened Coulomb (ECSC) potential. Roothaan's approach is implemented for these models after solving the inherent difficulties to evaluate integrals where screening appears explicitly. A corresponding computer code was developed using the method of global basis sets (GBS). The reliability of this approach was verified by solving the Hartree-Fock equations through implementation of the finite-differences and finite-element grid methods and applied to two-electron atoms, yielding excellent agreement with the Roothaan-GBS (RGBS) method. The RGBS method was used to study the energy evolution and ionization threshold of several closed- and open-shell many-electron atoms embedded either in weak or strong DHS or ECSC plasma conditions. In all cases, a critical value of the screening length is obtained for which ionization is achieved, being systematically larger for DHS conditions, indicating the effect of a more repulsive ECSC potential. For He-like atoms in the ground state, we report a comprehensive set of accurate total energy data as a function of the screening constant using the Lagrange mesh method, which includes the electron correlation effects. The electron correlation energy is estimated using this data with reference to the RGBS estimates of energy as the Hartree-Fock energy. The variation of correlation energy as a function of screening constant under the different plasma potentials is rationalized in terms of a conjectured comparison theorem. Finally, a discussion on the effect of plasma strength on localization or delocalization of the electronic density derived from the RGBS method is presented in terms of changes in the Shannon entropy, yielding consistent results for delocalization close to the ionization threshold.

I. INTRODUCTION

The study of the electronic structure of atoms immersed in a plasma is important in several fields of physics where the systems are submitted to extreme conditions [1–4]. For this purpose, there are some plasma models to solve the corresponding Schrödinger equation. Under the dilute plasma environment, the Debye-Hückel screening (DHS) potential [5] has been used to model the screened Coulomb potential by introducing a short-range exponentially decaying function in to the electron-electron and electron-nucleus interaction. A variant of this potential, suitable for the dense plasma environment, is obtained by including a cosine function to obtain the exponential cosine screened Coulomb (ECSC) potential [4,6]. These two potentials are representative in plasma studies. These potentials are used to build the Hamiltonian for an atom immersed in a plasma and the solutions to the corresponding Schrödinger equation are sought. Within a given plasma potential, interesting effects of its depth (given by the nuclear charge) and the width (represented by a screening constant) on the electronic density and energy of the atomic states needs to be accurately assessed. Understanding the process of electronic charge transfer, including the behavior of electron density near the ionization threshold under different model potentials, is of fundamental importance in the theory of electronic structure and its applications. Considering that the experimental first ionization potential for all neutral atoms in the periodic table is bracketed just within ≈1 eV and the electron affinities are covered within ≈0.5 eV, it becomes essential to develop computational methods to solve the Schrödinger equation with high degree of numerical accuracy. To the best of our knowledge, the plasma model potentials have been mostly applied on atoms and molecules containing only a small number of electrons [7,8]. For example, for two-electron atoms there are reports of energy orbitals, cross sections, or ionization energies as function of a screening parameter [9–14]. Some of these studies rest on accurate or approximate methods. However, all of them show difficulties in evaluating

*jgo@xanum.uam.mx
†kalidas.sen@gmail.com

some integrals where the screening appears explicitly [15]. This is the main reason why there are no reports on the electronic structure of many-electron atoms in the periodic table in the presence of the DHS and ECSC potentials.

Hartree-Fock (HF) [16] and Kohn-Sham (KS) [17] are two of the main computational methods to address the problem of the electronic structure of systems involving a Coulomb screening. In our opinion, the main issue is related to the evaluation of integrals where the screening is involved and its corresponding implementation in computational codes. It is worthwhile to develop reliable and robust computational methods to solve HF or KS equations in the presence of the Coulomb screening potential, which can be useful to obtain the wave function or electron density and estimate other properties of an electronic system. In particular, for the study of the electron correlation energy defined as the the difference between the exact and HF total energies, $E_{exact} - E_{HF}$, the code development to implement the HF model assumes a special significance within the wave functional theory.

The aim of this article is twofold. First, we solve the HF equations when DHS and ECSC potentials are used as plasma models, to show how the Roothaan's approach is implemented for these problems. Further, we report accurate numerical results including the electron correlation for the He, Li$^+$, and Be^{2+} atoms in the ground state under the DHS and ECSC potentials using the Lagrange mesh method (LMM). We employ the corresponding HF energies using the RGBS method to estimate the electron correlation energy as a function of screening parameter for these atoms under the different plasma potentials. We show that the general trends in the variation of total energy between the two model potentials can be rationalized in terms of a recently proposed conjecture [13] for the multielectronic atoms derived from the comparison theorem of quantum mechanics. Finally, in the second part, we present a HF (RGBS) study of the multielectron atoms Li, Be, Ne, Na, Ar, and K as they approach the threshold ionization. For these atoms, the response of the electron density under the two different model screening potentials is in terms of the critical screening constant b, electron density difference at the nucleus, and the difference in Shannon information entropy. Atomic units (a.u.) are used throughout our work, unless physical units are stated explicitly.

II. THEORY

The Hamiltonian, $\hat{H}$, considered in this work, for many-electron atoms has the form

$$\hat{H} = \sum_{i=1}^{N} \left(-\frac{1}{2}\nabla_i^2 \right) + \sum_{i=1}^{N} v(\mathbf{r}_i) + \sum_{i>j}^{N} \sum_{j=1}^{N} V(\mathbf{r}_i, \mathbf{r}_j), \quad (1)$$

where N represents the number of electrons in the system. In this article, we do use two models for the interaction between charged particles. The first one is the DHS potential where

$$v(\mathbf{r}_i) = -\frac{Z}{r_i}e^{-br_i}, \quad (2)$$

and

$$V(\mathbf{r}_i, \mathbf{r}_j) = \frac{1}{|\mathbf{r}_j - \mathbf{r}_i|}e^{-b|\mathbf{r}_j - \mathbf{r}_i|}, \quad (3)$$

with $b = 1/\lambda$, λ is the screening length, and Z represents the nuclear charge.

The ECSC potential is another plasma model considered in this article; for this model, we have

$$v(\mathbf{r}_i) = -\frac{Z}{r_i}e^{-br_i}\cos(br_i) \quad (4)$$

and

$$V(\mathbf{r}_i, \mathbf{r}_j) = \frac{1}{|\mathbf{r}_j - \mathbf{r}_i|}e^{-b|\mathbf{r}_j - \mathbf{r}_i|}\cos(b|\mathbf{r}_j - \mathbf{r}_i|). \quad (5)$$

For the DHS potential, the Debye screening length, λ, is related to the density of the plasma electrons, temperature, and effective charge of the ions in the embedded plasma [5,18,19]. For the ECSC potential, λ is related to the electron wave number and the electron plasma frequency [4,20]. In this work, we use b as a parameter to describe the screening length for DHS and ECSC potentials and we will discuss its connection with the ionization potential.

A. Hartree-Fock approach

Within the Hartree-Fock (HF) approach, the wave function is modeled by a Slater determinant, which is built by spin orbitals. Each spin orbital represents an electron from the definition $\chi(\mathbf{x}) = \psi(\mathbf{r})\sigma(\omega)$, with $\sigma(\omega)$ being the $\alpha(\omega)$ spin or $\beta(\omega)$ spin wave function. The total energy associated to this wave function is obtained from

$$E = T + V_{ne} + V_{ee}, \quad (6)$$

with

$$T = \sum_{i=1}^{N} \left\langle \chi_i \left| -\frac{1}{2}\nabla^2 \right| \chi_i \right\rangle, \quad (7)$$

$$V_{ne} = \sum_{i=1}^{N} \langle \chi_i | v | \chi_i \rangle, \quad (8)$$

and

$$V_{ee} = \frac{1}{2}\sum_{i=1}^{N}\sum_{j=1}^{N} \langle \chi_i\chi_j || \chi_i\chi_j \rangle. \quad (9)$$

The integrals involved in these expressions have the following definitions:

$$\left\langle \chi_i \left| -\frac{1}{2}\nabla^2 \right| \chi_i \right\rangle = \int d\mathbf{x}\,\chi_i^*(\mathbf{x})\left(-\frac{1}{2}\nabla^2 \right)\chi_i(\mathbf{x}),$$
$$= \int d\mathbf{r}\,\psi_i^*(\mathbf{r})\left(-\frac{1}{2}\nabla^2 \right)\psi_i(\mathbf{r}), \quad (10)$$

$$\langle \chi_i | v | \chi_i \rangle = \int d\mathbf{x}\,\chi_i^*(\mathbf{x})v(\mathbf{r})\chi_i(\mathbf{x}) = \int d\mathbf{r}\,\psi_i^*(\mathbf{r})v(\mathbf{r})\psi_i(\mathbf{r}), \quad (11)$$

$$\langle \chi_i\chi_j || \chi_i\chi_j \rangle = \langle \chi_i\chi_j | \chi_i\chi_j \rangle - \langle \chi_i\chi_j | \chi_j\chi_i \rangle, \quad (12)$$

with

$$\langle \chi_i\chi_j | \chi_i\chi_j \rangle$$
$$= \iint d\mathbf{x}_1 d\mathbf{x}_2\,\chi_i^*(\mathbf{x}_1)\chi_j^*(\mathbf{x}_2)\chi_i(\mathbf{x}_1)\chi_j(\mathbf{x}_2)V(\mathbf{r}_1, \mathbf{r}_2)$$
$$= \iint d\mathbf{r}_1 d\mathbf{r}_2\,|\psi_i(\mathbf{r}_1)|^2|\psi_j(\mathbf{r}_2)|^2 V(\mathbf{r}_1, \mathbf{r}_2), \quad (13)$$

and

$$\langle \chi_i \chi_j | \chi_j \chi_i \rangle$$
$$= \iint d\mathbf{x}_1 d\mathbf{x}_2 \chi_i^*(\mathbf{x}_1) \chi_j^*(\mathbf{x}_2) \chi_j(\mathbf{x}_1) \chi_i(\mathbf{x}_2) V(\mathbf{r}_1, \mathbf{r}_2)$$
$$= \iint d\mathbf{r}_1 d\mathbf{r}_2 \psi_i^*(\mathbf{r}_1) \psi_j^*(\mathbf{r}_2) \psi_j(\mathbf{r}_1) \psi_i(\mathbf{r}_2) V(\mathbf{r}_1, \mathbf{r}_2)$$
$$\times \int d\omega_1 \sigma_i^*(\omega_1) \sigma_j(\omega_1) \int d\omega_2 \sigma_j^*(\omega_2) \sigma_i(\omega_2). \quad (14)$$

Orbitals that minimize the total energy must satisfy the HF equations [16]

$$\left(-\frac{1}{2} \nabla_1^2 + v(\mathbf{r}_1) + \sum_{a=1}^{N} [J_a - K_a] \right) \chi_i(\mathbf{x}_1) = \epsilon_i \chi_i(\mathbf{x}_1), \quad (15)$$

with

$$J_a(\mathbf{x}_1) \chi_i(\mathbf{x}_1) = \left[\int d\mathbf{x}_2 \chi_a^*(\mathbf{x}_2) \chi_a(\mathbf{x}_2) V(\mathbf{r}_1, \mathbf{r}_2) \right] \chi_i(\mathbf{x}_1) \quad (16)$$

and

$$K_a(\mathbf{x}_1) \chi_i(\mathbf{x}_1) = \left[\int d\mathbf{x}_2 \chi_a^*(\mathbf{x}_2) \chi_i(\mathbf{x}_2) V(\mathbf{r}_1, \mathbf{r}_2) \right] \chi_a(\mathbf{x}_1). \quad (17)$$

Thus, we must solve Eq. (15) for each χ_i and the resulting orbitals are used to evaluate the total energy from Eq. (6).

B. The Lagrange mesh method

From Eqs. (1), (2), and (3), the helium-like atom under the DHS potential is given by the Schrödinger equation

$$\hat{H}_{\text{DHS}} = -\frac{1}{2} (\nabla_1^2 + \nabla_2^2) - Z \left(\frac{\exp(-br_1)}{r_1} + \frac{\exp(-br_2)}{r_2} \right)$$
$$+ \frac{\exp(-br_{12})}{r_{12}}. \quad (18)$$

We have employed the Lagrange-mesh method (LMM) [21–24] in which the Schrödinger equation, under the fully correlated electron-electron interactions, is placed into a nonuniform inhomogeneous lattice defined by zeros of classical orthogonal polynomials, using a basis of Laguerre functions and the associated Gauss quadratures. The details of this accurate computational procedure along with its diverse applications have been extensively reviewed in Ref. [25]. Very recently, LMM calculations have been reported for He-like atoms under a screened Coulomb potential, providing the accurate estimates of the critical nuclear charge [13,26,27]. The numerical calculations reported in the present work have been performed using the perilag code originally written by Baye and coworkers [21–25] for the three unscreened Coulomb charges. Here, the wave function is expressed in terms of the perimetric coordinates [28,29],

$$x = -r_1 + r_2 + r_{12},$$
$$y = r_1 - r_2 + r_{12},$$
$$z = r_1 + r_2 - r_{12},$$

which are all defined over $[0, \infty]$. Our version of the perilag code employs the JADAMILU program for fast diagonalization

of large sparse matrices [30]. The particular choice of the perimeric coordinates makes the perilag code easily adaptable to a continuous and analytic potential function, for example, the DHS potential. The straightforward modifications of the code to implement the DHS potential involves replacing the original unscreened potential with the exponential screening terms in all the three Coulombic interactions involving the radial variables r_1, r_2, and r_{12} as given in Eq. (18). We note here that the presently calculated LMM energies for He atom in the presence of the DHS potential agree up to six decimal places with those reported using a 308-term expansion in Hylleraas coordinates [13,26]. In addition, wherever available, the LMM energies are in quantitative agreement with the other accurate values for He reported in the literature [9,10]. For the Li$^+$ and Be^{2+} atoms, the presently reported values of energy, to our knowledge, present the most accurate values. For Li$^+$, our results are more accurate than those reported earlier [31].

III. TECHNICAL DETAILS

A. Hartree-Fock computation

To solve Eq. (15), it is convenient to use a spin-free equation by integration of the variable ω_1. Besides, for atoms, it is useful the following representation for each spatial orbital

$$\psi_i(\mathbf{r}) = R_i(r) Y_{\ell_i}^{m_i}(\Omega), \quad (19)$$

where $R_i(r)$ is the radial contribution and $Y_{\ell_i}^{m_i}(\Omega)$ represents the spherical harmonic functions. In this way, Eq. (15) is transformed into

$$-\frac{1}{2} \hat{O}_{r_1} R_i(r_1) + \frac{\ell(\ell+1)}{2r_1^2} R_i(r_1) + v(r_1) R_i(r_1)$$
$$+ \int d\Omega_1 Y_{\ell_i}^{m_i*}(\Omega_1) \int d\omega_1 \sigma_i^*(\omega_1) [J_a - K_a]$$
$$\times \sigma_i(\omega_1) R_i(r_1) Y_{\ell_i}^{m_i}(\Omega_1) = \epsilon_i R_i(r_1), \quad (20)$$

with

$$\hat{O}_r = \frac{\partial^2}{\partial r^2} + \frac{2}{r} \frac{\partial}{\partial r}. \quad (21)$$

For the Coulomb part, we have

$$\int d\Omega_1 Y_{\ell_i}^{m_i*}(\Omega_1) \int d\omega_1 \sigma_i^*(\omega_1) J_a \sigma_i(\omega_1) R_i(r_1) Y_{\ell_i}^{m_i}(\Omega_1)$$
$$= \left[\int d\mathbf{r}_2 \psi_a^*(\mathbf{r}_2) \psi_a(\mathbf{r}_2) V(\mathbf{r}_1, \mathbf{r}_2) \right] R_i(r_1). \quad (22)$$

For the exchange contribution, the corresponding expression for K_a depends on the electron configuration defined for an atom since some of these integrals are zero. In summary, we have to solve Eq. (20) to obtain $R_i(r)$. The integrals involved in this solution are an important issue in this procedure.

In our group, we have developed the MEXICA-C code to study confined many-electron atoms [32]. This code is based on the Roothaan's approach [16], where a global basis set (GBS) is used,

$$R_i(r) = \sum_{\mu=1}^{k} c_\mu^i f_\mu(r) = \sum_{\mu=1}^{k} c_\mu^i N_\mu r^{n_\mu - 1} e^{-\zeta_\mu r}, \quad (23)$$

TABLE I. Total and orbital energies in a.u. for the ground state ($1s^2$) of He, Li$^+$, and Be^{2+} without presence of the plasma environment.

	He	Li$^+$	Be^{2+}
E_{HF}	-2.86168000	-7.23641520	-13.61129943
	-2.86168000[a]	-7.23641520[a]	-13.61129942[b]
ϵ_{1s}	-0.91795540	-2.79236449	-5.66711560
	-0.91795555[b]	-2.79236440[b]	-5.66711560[b]
E_{LMM}	-2.90372438	-7.27991341	-13.65556624
	-2.90372438[a]	-7.27991341[a]	-13.65556623[c]

[a]Ref. [33]; [b]Ref. [34]; [c]Ref. [35].

which yields an algebraic problem to find the set of coefficients $\{c_\mu^i\}$. In Ref. [32], the reader can find details related to its implementation for confined atoms. Expressions of the integrals involved with DHS and ECSC potentials can be found in the Appendix. All these integrals have been implemented in MEXICA-C code to obtain the corresponding HF results.

B. The Lagrange mesh method computation

We have employed the lattice parameters [30] $N_x = N_y = 50$, $N_z = 40$, and the scaling parameters $h_x = h_y = 0.8$, $h_z = 0.5$.

IV. RESULTS

A. Two-electron atoms under plasma models

To check our implementation, we studied two-electron systems: He, Li$^+$, and Be^{2+}. The case of the helium-like ions allows one to show in detail the effects of the plasma medium on the ground-state energy and understand the multielectronic results found in this work. The results obtained by HF and LMM for He, Li$^+$, and Be^{2+} are reported in Table I for unconfined atoms, i.e., $b = 0$. From these results, we study the effect of the plasma on these atoms.

1. Hartree-Fock results for two-electron atoms embedded in a plasma

The results obtained for HF energy, E_{HF}, are summarized in Fig. 1. Specific values of E_{HF} as a function of the screening parameter b can be found in Table II.

We observe from Fig. 1 that the impact of the screening parameter of both plasma models is similar over the total energy when b is small (free case, no plasma environment). However, the cosine function involved in the ECSC potential induces an additional repulsive force, which is evidenced on the behavior of the total energy where the ECSC potential gives an energy above the results produced by the DHS model. Thus, the ECSC increases the total energy more quickly than the DHS potential for high values of b and consequently E_{HF} reaches zero more quickly with the ECSC potential.

Plasma effects are observed also over orbital energies, as evidenced in Fig. 2, where the orbital energy, ϵ_{1s}, is presented as a function of b. From this figure, we appreciate that for a fixed ϵ_{1s}, the DHS potential needs a b bigger than that presented by the ECSC potential to account for the same orbital
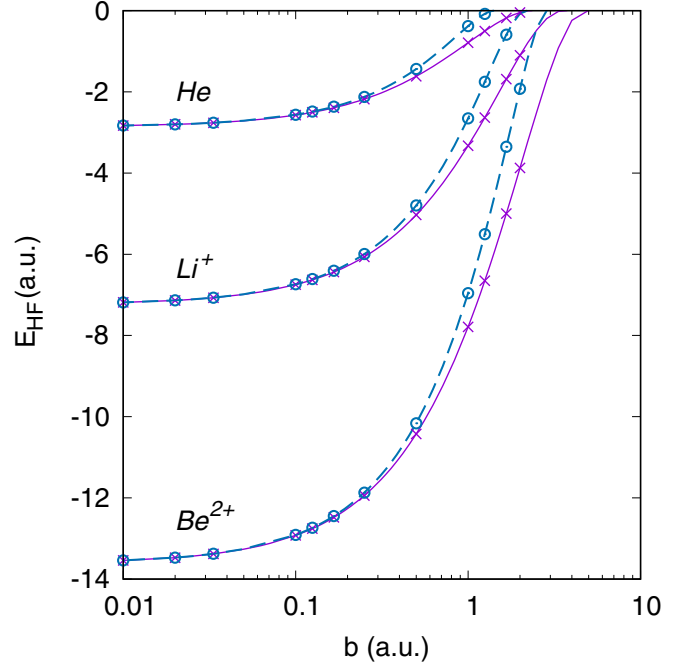

FIG. 1. Hartree-Fock total energy (E_{HF}), in atomic units, for He, Li$^+$, and Be^{2+} considering two plasma models: (a) DHS (solid lines with crosses) and (b) ECSC (dashed line with circles).

energy. Thus, for this property, we corroborate the repulsive character of the cosine function involved in the ECSC plasma model. Within the HF method, the interpretation of the highest occupied atomic orbital, ϵ_{1s}, is given by Koopmans' theorem to estimate the ionization potential, I, through the relation
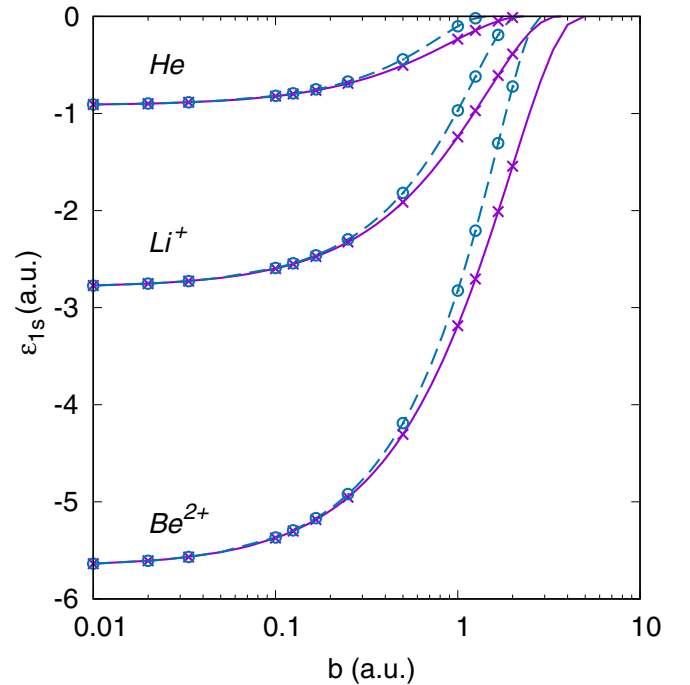

FIG. 2. $1s$ occupied atomic orbital energy (ϵ_H), in atomic units, for He, Li$^+$, and Be^{2+} considering two plasma models: (a) DHS (solid lines and crosses) and (b) ECSC (dashed line and circles).

TABLE II. Hartree-Fock (E_{HF}) and Lagrande mesh method (E_{LMM}) energies in a.u. for He, Li$^+$, and Be^{2+} atoms embedded in two plasma models: (a) Debye-Hückel screening (DHS) potential and (b) exponential cosine screened Coulomb (ECSC) potential.

	DHS		ECSC	
b	E_{HF}	E_{LMM}	E_{HF}	E_{LMM}
		He		
0.00	−2.86168000	−2.90372438	−2.86168000	−2.90372438
0.01	−2.83179695	−2.87383879	−2.83168078	−2.87372513
0.02	−2.80214627	−2.84418058	−2.80168624	−2.84373033
0.05	−2.71456596	−2.75654881	−2.71177590	−2.75381581
0.10	−2.57304480	−2.61485295	−2.56242532	−2.60443557
0.20	−2.30582711	−2.34700618	−2.26731385	−2.30911417
0.30	−2.05835487	−2.09862877	−1.97969172	−2.02101851
0.40	−1.82924600	−1.86845055	−1.70224716	−1.74285188
0.50	−1.61731891	−1.65540132	−1.43720300	−1.47695782
0.60	−1.42153378	−1.45855793	−1.18644936	−1.22546957
0.70	−1.24095212	−1.27710900	−0.95162140	−0.99043071
0.80	−1.07470790	−1.11033009	−0.73413066	−0.77390048
0.90	−0.92198643	−0.95756547	−0.53515646	−0.57805164
1.00	−0.78200897	−0.81821418	−0.35560267	−0.40526123
		Li$^+$		
0.00	−7.23641520	−7.27991341	−7.23641520	−7.27991341
0.01	−7.18654470	−7.23004184	−7.18641579	−7.22991399
0.02	−7.13693203	−7.18042597	−7.13641991	−7.17991804
0.05	−6.98962383	−7.03309572	−6.98648788	−7.02998485
0.10	−6.74911134	−6.79250671	−6.73698462	−6.78047319
0.20	−6.28616252	−6.32926775	−6.24078692	−6.28421255
0.30	−5.84619377	−5.88884627	−5.75059269	−5.79386079
0.40	−5.42802377	−5.47008214	−5.26875708	−5.31174355
0.50	−5.03062137	−5.07196244	−4.79731188	−4.83987293
0.60	−4.65307483	−4.69359111	−4.33804460	−4.38002450
0.70	−4.29456922	−4.33416683	−3.89256451	−3.93380128
0.80	−3.95436946	−3.99296642	−3.46235785	−3.50268728
0.90	−3.63180712	−3.66933195	−3.04883503	−3.08809382
1.00	−3.32626993	−3.36266070	−2.65337235	−2.69140135
		Be^{2+}		
0.00	−13.61129943	−13.65556624	−13.6112994	−13.6555662
0.01	−13.54143456	−13.58570078	−13.5412999	−13.5855667
0.02	−13.47183905	−13.51610351	−13.4713031	−13.5155699
0.05	−13.26465510	−13.30890741	−13.2613565	−13.3056228
0.10	−12.92461213	−12.96882195	−12.9117486	−12.9560115
0.20	−12.26371301	−12.30775948	−12.2147816	−12.2590182
0.30	−11.62746051	−11.67124775	−11.5226947	−11.5668640
0.40	−11.01484162	−11.05828309	−10.8375089	−10.8815551
0.50	−10.42494849	−10.46796597	−10.1610137	−10.2048693
0.60	−09.85696075	−09.89948343	−09.4948064	−09.5383953
0.70	−09.31013171	−09.35209544	−08.8403282	−08.8835682
0.80	−08.78377754	−08.82512416	−08.1988952	−08.2416997
0.90	−08.27726853	−08.31794528	−07.5717250	−07.6140050
1.00	−07.79002187	−07.82998099	−06.9599607	−07.0016262

$I \approx -\epsilon_{1s}$ [36]. In this context, Fig. 2 gives important information about the ionization of two-electron systems. From this figure, we observe the impact of a plasma environment over the ionization potential, which is reduced when b is increased; in fact, there is one value of b where $\epsilon_{1s} = 0$, indicating that under this circumstance the atom is ionized. This critical value

TABLE III. Critical screening parameter, b_{crit}, for ionization threshold of several atomic systems embedded in a plasma with DHS and ECSC screening. Corresponding values of change in information entropy, ΔS_ρ, and change in electron density, $\Delta \rho(0)$, are also reported (see text). All quantities in a.u.

	DHS			ECSC		
Atom	b_{crit}	ΔS_ρ	$\Delta \rho(0)$	b_{crit}	ΔS_ρ	$\Delta \rho(0)$
Be^{2+}	4.72	21.22	−33.92	2.87	24.68	−33.83
Li$^+$	3.55	23.77	−13.56	2.15	22.37	−13.35
He	2.33	17.36	−3.51	1.42	17.02	−3.40
Li	0.47	6.94	−0.58	0.26	6.07	−0.14
Be	0.78	14.07	−2.65	0.43	12.07	−0.99
Ne	1.10	12.68	−9.71	0.77	7.32	0.43
Na	0.40	7.33	−2.35	0.23	5.09	−0.28
Ar	0.74	14.38	−15.23	0.49	7.70	2.21
K	0.29	4.46	−9.73	0.17	2.17	−6.37

of the screening parameter, b_{crit}, is reported in Table III. From Table III, we observe an important difference between DHS and ECSC screening models; the cosine function involved in the ECSC is more repulsive than DHS and consequently the corresponding b_{crit} is bigger in DHS potential than that presented by the ECSC potential. We are now presenting a rationalization of these trends by invoking a conjecture based on the comparison theorem of quantum mechanics [13] valid for the multielectronic atoms. This will be followed by a similar analysis of the correlation energy obtained as the difference between the energy calculated using the LMM and the HF method, $E_{LMM} - E_{HF}$.

2. The correlation energy in the DHS and ECSC potentials: Ground state He-like atoms

The elementary comparison theorem of quantum mechanics states that if two spherically symmetric one-electron potentials are ordered, $v^{(1)}(r) \geqslant v^{(2)}(r)$, then their corresponding pairs of eigenvalues, for all n, ℓ, are ordered, $E_{n,\ell}^{(1)} \geqslant E_{n,\ell}^{(2)}$. For nonrelativistic Hamiltonians bounded from below, this theorem is a direct consequence of the variational characterization of the eigenspectrum [37–39]. *Generalized* comparison theorems have been proposed [40,41] which admit the two potential curves to cross over in a controlled fashion while maintaining a definite ordering of the respective eigenvalues. *Refined* comparison theorems applicable to the relativistic Dirac Hamiltonian have been also reported [42–44].

A concise summary of the work done on the comparison theorem is available in Refs. [45,46]. The conjectured comparison theorem obtained [13] in a series of plasma potentials as applied in the present context leads to $E_{DHS} < E_{ECSC}$. We note here that this relative ordering of energy levels holds good for both the HF and LMM estimates. The numerical results for the HF data have been already presented in Fig. 1, which validate the conjectured comparison theorem. In Fig. 3, we have similarly compared the LMM estimates of energy for the He, Li$^+$, and Be^{2+} atoms in their ground state, and the corresponding data are reported in Table II. It is found that
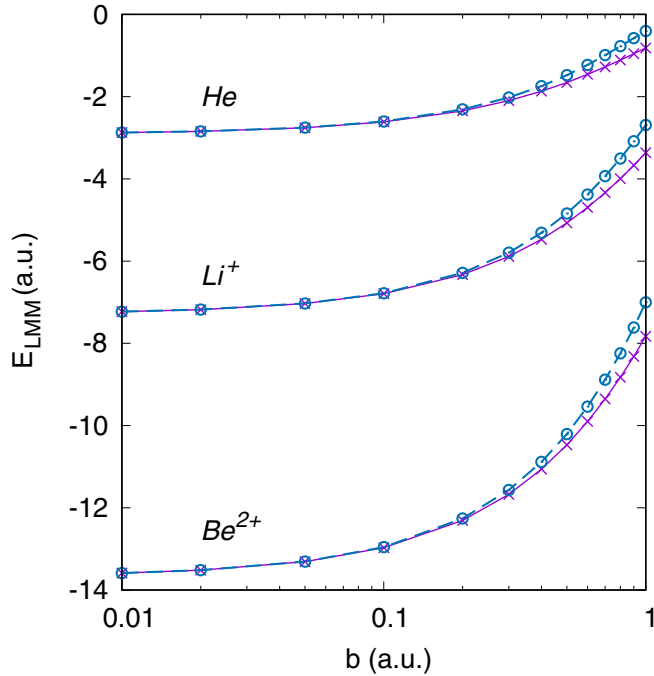
FIG. 3. Lagrange mesh method total energy ($E_{\rm LMM}$), in atomic units, for He, Li$^+$, and Be^{2+} considering two plasma models: (a) DHS (solid lines with crosses) and (b) ECSC (dashed line with circles).

the relative ordering of the energy levels is given by $E_{\rm DHS} < E_{\rm ECSC}$. A direct consequence of the trends observed in Figs. 1 and 3, namely the difference $E_{\rm DHS} - E_{\rm ECSC}$ in the HF case is found to be below that of the LMM estimates, gives rise to
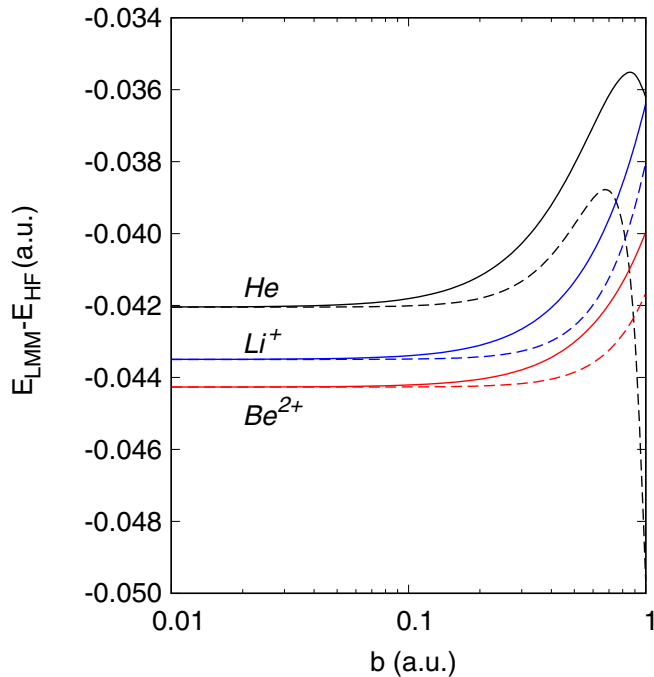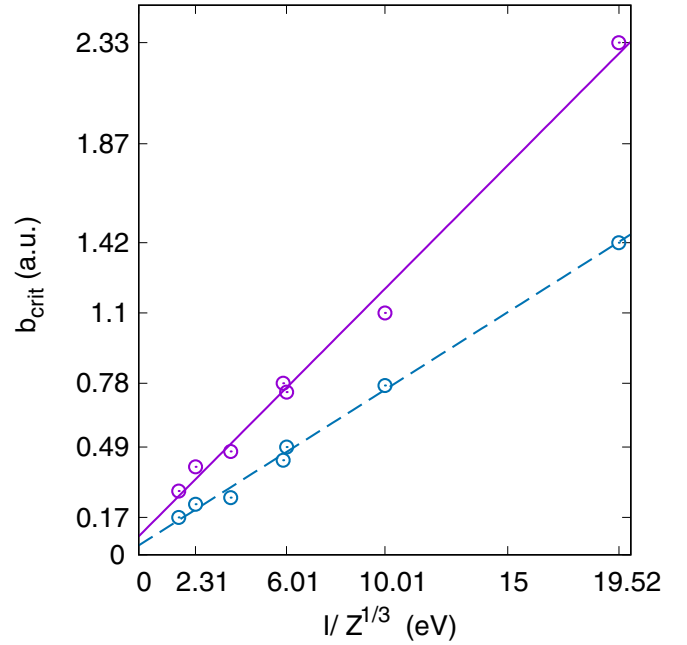

FIG. 4. $E_{\rm LMM}$-$E_{\rm HF}$ energy difference, in atomic units, for He, Li$^+$, and Be^{2+} considering two plasma models: (a) DHS (solid lines) and (b) ECSC (dashed line).

FIG. 5. Linear relationship $b_{\rm crit} = mIZ^{-1/3} + k$, with I as the ionization potential and Z as the nuclear charge. (a) DHS model (solid line) with $m = 0.1125$ au/eV, $k = 0.0837$ au, and correlation coefficient of 0.9928. (b) ECSC model (dashed line) with $m = 0.0708$ au/eV, $k = 0.0438$ au, and correlation coefficient of 0.9960. Free atom values of the ionization potential values from NIST Atomic Spectra Database Ionization Energies Form [47].

the ordering of the electron correlation energy, $E_{\rm Corr}$, defined as $E_{\rm LMM} - E_{\rm HF}$, according to $E_{\rm Corr-ECSC} < E_{\rm Corr-DHS}$. This is vindicated by the plot of correlation energy versus b shown in Fig. 4. Furthermore, we observe that as b increases, the difference becomes larger, that is, correlation effects are more important for stronger plasma, as well as when the electrons reach the ionization threshold.

B. Ionization by the action of a plasma in many-electron atoms

The effects presented by two-electron atoms when they are immersed in a plasma are also observed in many-electron atoms. In the same Table III, we do report the $b_{\rm crit}$ for several noble gases, alkali atoms, and Be. We must mention that MEXICA-C has implemented the unrestricted HF (UHF) method to solve the corresponding HF equations for open-shell atoms, e.g., alkali atoms. All atoms considered in this article exhibit the same difference between DHS and ECSC potentials; ECSC induces b smaller than DHS. We found an important result: $b_{\rm crit}^{\rm alkali} < b_{\rm crit}^{\rm noble\ gases}$. This result is connected with the ionization potential presented by alkali atoms and noble gases in the periodic table, since this behavior is mapped over values of b to eject an electron in a plasma. We observe that the neutral K atom presents the lowest $b_{\rm crit}$ and He the highest one. The behavior delivered by $b_{\rm crit}$ in this table suggests a relationship between this quantity and I reported for free atoms. Thus, by considering the periodicity of I through the coefficient $Z^{-1/3}$ [47], we have a nice linear relationship between $IZ^{-1/3}$ and $b_{\rm crit}$, as corroborated in Fig. 5. In
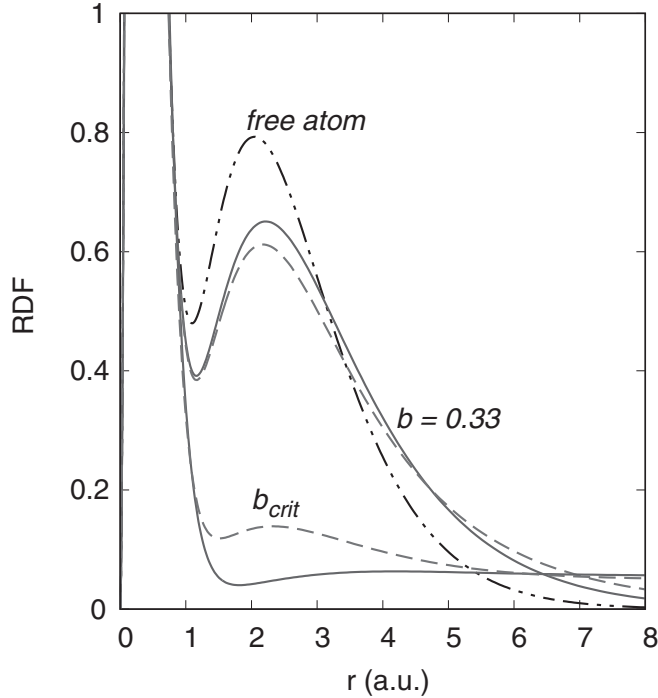
FIG. 6. Radial distribution function as obtained by the GBS approach for free beryllium atom (dot-dot-dashed line) and considering two plasma models: (a) DHS (solid lines) and (b) ECSC (dashed lines).
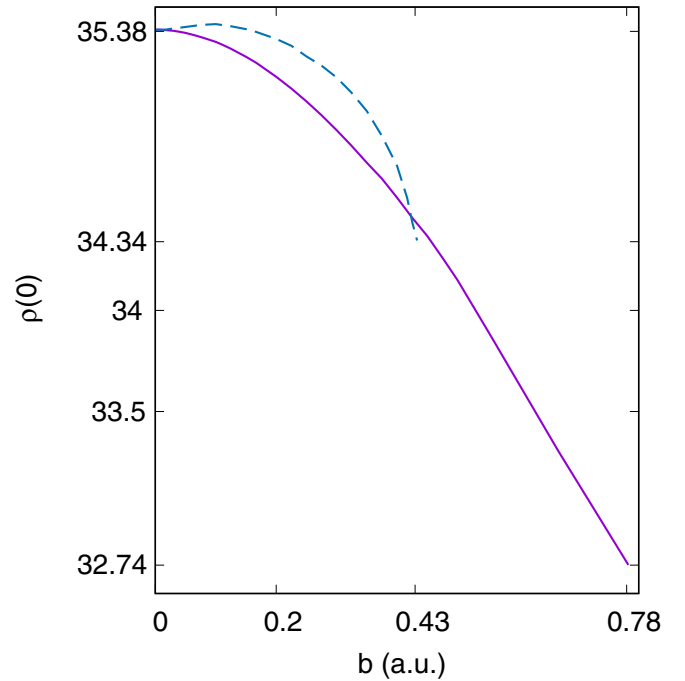

FIG. 7. Electron density evaluated at the origin of the beryllium atom considering two plasma models: (a) DHS (solid lines) and (b) ECSC (dashed lines).

conclusion, b_{crit} is connected with I. We have included results for alkali and noble gas atoms since they are representative of the ionization potential in the periodic table. Therefore, in this table we are reporting upper and bottom bounds for b for some periods in the periodic table. Naturally, the linear relationships from Fig. 5 are useful. For example, the NIST Atomic Spectra Database Ionization Energies Form [48] reports for magnesium $I = 7.65$ eV; from the linear relationships of Fig. 5, we predict that $b_{crit} = 0.46$ au and 0.28 au for DHS and ECSC models, respectively. We must mention that the exponent's optimization in the basis set for Roothaan's approach is computationally expensive, and for that reason, we do not report b_{crit} for the whole periodic table.

We have included the beryllium atom in Table III since this atom presents interesting characteristics when it is confined by a constant potential, which induces ionization for particular confinement values. For this reason, we think it is convenient to analyze this atom under the action of the plasma models considered here. We present the radial distribution function (RDF) of the electron density in Fig. 6 for several values of b. By using the free atom as the reference, we observe that the most external maximum decreases when b is increased. The behavior of this local property is quite similar to that found in our laboratory for beryllium confined by a finite potential. For both plasma models, we found that for confinements where the atom is almost ionized, the electron density is spread out over the whole space. This effect is mapped also over the electron density evaluated at the nucleus, $\rho(0)$, through the difference $\Delta\rho(0) = \rho_{Plasma}(0) - \rho_{free}(0)$, which is reported in Table III. Thus, we observe that when the atom is almost

ionized by a plasma, the electron density presents a reduction at the nucleus since part of this charge distribution has been delocalized. This is true for the DHS model for all atoms. For the ECSC model, there are two exceptions of this behavior, Ne and Ar; for these atoms, the electron density is localized close to the nucleus. Therefore, the confinement imposed by ECSC model predicts different results than those found by using the DHS model or a constant potential.

We have tracked the behavior of $\rho(0)$ as a function of b. This behavior is presented in Fig. 7 for the beryllium atom embedded in the DHS and ECSC plasma models. This figure reveals an important difference between ECSC and DHS models. For the DHS model, $\rho(0)$ always decreases when b is increased. However, for the ECSC model, $\rho(0)$ increases for some values of b. This result indicates that for some values of b the ECSC model localizes the electron density. In contrast, the electron density always is delocalized when b is increased in the DHS model. This result confirms that the ECSC potential is more repulsive than that imposed by the DHS potential.

Localization or delocalization of the electron density for confined atoms [49–53] has been studied through the Shannon entropy [54], defined as

$$S_\rho = -\int \rho(\mathbf{r}) \ln \rho(\mathbf{r}) d\mathbf{r}. \tag{24}$$

We consider that this quantity, useful in information theory field, is appropriate to measure the localization or delocalization of the electron density when atoms are confined [51,53], in particular by a plasma. The Shannon entropy for beryllium confined by DHS and ECSC potentials is presented in Fig. 8. For this plot, we used the spherical average of the
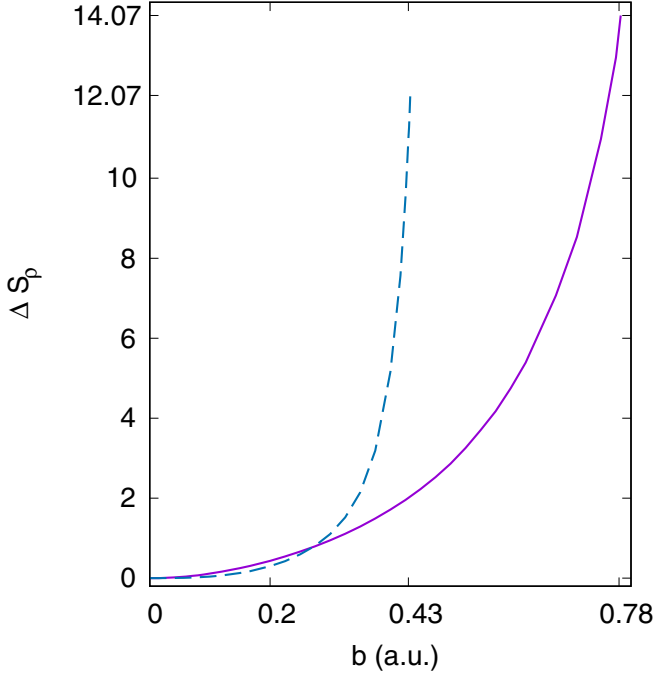
FIG. 8. Shannon entropy difference of the beryllium atom as a function of the plasma screening parameter as obtained by considering two plasma models: (a) DHS (solid lines) and (b) ECSC (dashed lines).

electron density, as in other reports [55]. In previous works, the difference $\Delta S_\rho = S_\rho^{\text{conf}} - S_\rho^{\text{free}}$ has been used as a measure of localization, $\Delta S_\rho < 0$, or delocalization $\Delta S_\rho > 0$ of the electron density [51,53]. We observe, from Fig. 8, that ΔS_ρ grows up rapidly when b is close to b_{crit}, indicating that for these values of b the electron density is delocalized. ΔS_ρ for b_{crit} is reported in Table III for the atoms considered in this article. From here, it is evident that this quantity is large when an electron is almost ejected from an atom by the action of a plasma.

V. CONCLUSIONS

In this article, we studied several closed- and open-shell atoms embedded in a plasma by means of two plasma models: the Debye-Hückel and an exponential cosine screened Coulomb potential. For both cases, the Hartree-Fock equations were solved by using a global basis set through the Roothaan's approach. The coupling strength associated to the plasma environment was varied until each atom was ionized. We found that this critical coupling strength has a direct relationship with the experimental ionization energy of each atom. Such a relationship is able to predict the critical coupling strength of neutral atoms from their corresponding ionization potential. We found that within a plasma when an atom is almost ionized, its electron density is delocalized and this behavior is corroborated by using the Shannon entropy since this property is increased rapidly under this circumstance. Finally, the theoretical estimates of electron correlation energy for the He-like atoms in the ground state are found to be ordered as the exponential cosine screened Coulomb potential staying below the corresponding Debye-Hückel screening potential,

in validation of a conjectured comparison theorem for the multielectronic atoms.

APPENDIX: MATRIX ELEMENTS OF ROOTHAAN'S APPROACH

Because of the electron interaction with the plasma medium, the screening potential $V(\mathbf{r}_1, \mathbf{r}_2)$ adds an angular dependence. For example, for the DHS potential, Eq. (3) is rewritten as [4,11,15]

$$V(\mathbf{r}_1, \mathbf{r}_2) = \frac{1}{|\mathbf{r}_1 - \mathbf{r}_2|} e^{-b|\mathbf{r}_1 - \mathbf{r}_2|}, \tag{A1}$$

$$= -b \sum_{\ell=0}^{\infty} (2\ell + 1) j_\ell(ibr_<) h_\ell^{(1)}(ibr_>) P_\ell(\cos\theta), \tag{A2}$$

where $r_< = \min(r_1, r_2)$, $r_> = \max(r_1, r_2)$, θ is the angle between $\mathbf{r}_1$ and $\mathbf{r}_2$, $P_\ell(x)$ are the Legendre polynomials, $j_\ell(x)$ are the spherical Bessel functions, and $h_\ell(x)$ are the Hankel functions of first kind for a given angular momentum number ℓ. In the case of ECSC potential, Eq. (5), the cosine term is expanded as a function of a sum of two exponential terms using Eq. (A1) twice [15].

Integrals in the HF method can be separated into radial and angular contributions. For the angular contribution, we used the Clebsch-Gordan coefficients and for the radial part we found integrals with the expression

$$I_{\text{DHSP}} = \int dr \frac{r_1^p r_2^q e^{-\alpha r_1} e^{-\beta r_2} e^{-|\mathbf{r}_2 - \mathbf{r}_1|/\lambda}}{|\mathbf{r}_2 - \mathbf{r}_1|}, \tag{A3}$$

$$I_{\alpha\beta pq}^{(\ell,b)} = \int_0^\infty \int_0^\infty r_1^p r_2^q e^{-\alpha r_1 - \beta r_2} j_\ell(ibr_<) h_\ell^{(1)}(ibr_>) dr_1 dr_2, \tag{A4}$$

and

$$I_{\text{ECSCP}} = \int dr \frac{r_1^p r_2^q e^{-\alpha r_1} e^{-\beta r_2} e^{-|\mathbf{r}_2 - \mathbf{r}_1|/\lambda}}{|\mathbf{r}_2 - \mathbf{r}_1|} \cos(|\mathbf{r}_2 - \mathbf{r}_1|/\lambda), \tag{A5}$$

where q and p are integers and α and β are real. In this case, the integral $I_{\alpha\beta pq}^{(\ell,b)}$ has a closed form

$$I_{\alpha\beta pq}^{(\ell,b)} = H_{\alpha\beta pq}^{(\ell,b)} + G_{\alpha\beta pq}^{(\ell,b)} \tag{A6}$$

with

$$H_{\alpha\beta pq}^{(\ell,b)} = \sum_{m=0}^{\ell} \frac{(\ell+m)!}{2^m m!(\ell-m)!b^{m+1}} \sum_{\kappa=0}^{\ell} \frac{(\ell+\kappa)!(p-\kappa-1)!}{\kappa!(\ell-\kappa)!(2b)^{\kappa+1}}$$

$$\times \left[\frac{(q-m-1)!}{(\beta+b)^{q-m}} \left(\frac{(-1)^{\kappa}}{(\alpha-b)^{p-\kappa}} + \frac{(-1)^{\ell+1}}{(\alpha+b)^{p-\kappa}} \right) \right.$$

$$- \sum_{s=0}^{p-\kappa-1} \frac{(q+s-m-1)!}{s!} \left(\frac{(-1)^{\kappa}}{(\alpha-b)^{p-s-\kappa}(\alpha+\beta)^{q+s-m}} \right.$$

$$\left. \left. + \frac{(-1)^{\ell+1}}{(\alpha+b)^{p-s-\kappa}(\alpha+\beta+2b)^{q+s-m}} \right) \right], \qquad \text{(A7)}$$

and

$$G_{\alpha\beta pq}^{(\ell,b)} = \sum_{m=0}^{\ell} \frac{(\ell+m)!}{m!(\ell-m)!(2b)^{m+1}}$$

$$\times \sum_{\kappa=0}^{\ell} \frac{(\ell+\kappa)!(p-\kappa-1)!}{2^{\kappa}\kappa!(\ell-\kappa)!b^{\kappa+1}(\alpha+b)^{p-\kappa}}$$

$$\times \sum_{s=0}^{q-\kappa-1} \frac{(\alpha+b)^s(q+s-m-1)!}{s!} \left(\frac{(-1)^m}{(\alpha+\beta)^{q+s-m}} \right.$$

$$\left. + \frac{(-1)^{\ell+1}}{(\alpha+\beta+2b)^{q+s-m}} \right). \qquad \text{(A8)}$$

[1] F. Graziani, M. Desjarlais, R. Redmer, and S. Trickey, eds., *Frontiers and Challenges in Warm Dense Matter*, Lecture Notes in Computational Science and Engineering Vol. 96 (Springer, Cham, 2014).

[2] D. Salzmann, ed., *Atomic Physics in Hot Plasmas* (Oxford University Press, Oxford, UK, 1998), p. 272.

[3] M. S. Murillo and J. C. Weisheit, Phys. Rep. **302**, 1 (1998).

[4] R. K. Janev, S. Zhang, and J. Wang, Matt. Rad. Extrem. **1**, 237 (2016).

[5] P. Debye and E. Hückel, Phys. Z. **24**, 185 (1923).

[6] P. Shukla and B. Eliasson, Phys. Lett. A **372**, 2897 (2008).

[7] B. Saha and S. Fritzsche, Phys. Rev. E **73**, 036405 (2006).

[8] J. Deprince, M. A. Bautista, S. Fritzsche, J. A. García, T. R. Kallman, C. Mendoza, P. Palmeri, and P. Quinet, Astron. Astrophys. **643**, A57 (2020).

[9] S. Kar and Y. K. Ho, Int. J. Quantum Chem. **106**, 814 (2006).

[10] A. Ghoshal and Y. K. Ho, J. Phys. B: At. Mol. Opt. Phys. **42**, 075002 (2009).

[11] M. C. Zammit, D. V. Fursa, I. Bray, and R. K. Janev, Phys. Rev. A **84**, 052705 (2011).

[12] Y.-C. Lin, T.-K. Fang, and Y. K. Ho, Phys. Plasmas **22**, 032113 (2015).

[13] K. D. Sen, J. Katriel, and H. E. Montgomery, Ann. Phys. **397**, 192 (2018).

[14] S. Kar, Y.-S. Wang, and Y. K. Ho, Phys. Rev. A **99**, 042514 (2019).

[15] L. G. Jiao, L. R. Zan, L. Zhu, J. Ma, and Y. K. Ho, Comput. Phys. Commun. **244**, 217 (2019).

[16] A. Szabo and N. S. Ostlund, *Modern Quantum Chemistry: Introduction to Advanced Electronic Structure Theory* (Dover, New York, 1996).

[17] R. G. Parr and W. Yang, *Density-Functional Theory of Atoms and Molecules* (Oxford University Press, Oxford, UK, 1994).

[18] National Research Council, *Plasma Science: From Fundamental Research to Technological Applications* (The National Academies Press, Washington, DC, 1995), p. 224.

[19] A. Sil, S. Canuto, and P. Mukherjee, Adv. Quantum Chem. **58**, 115 (2009).

[20] Y. Y. Qi, J. G. Wang, and R. K. Janev, Phys. Plasmas **24**, 062110 (2017).

[21] D. Baye and P.-H. Heenen, J. Phys. A **19**, 2041 (1986).

[22] M. Hesse and D. Baye, J. Phys. B **32**, 5605 (1999).

[23] M. Hesse and D. Baye, J. Phys. B **34**, 1425 (2001).

[24] D. Baye and K. D. Sen, Phys. Rev. E **78**, 026701 (2008).

[25] D. Baye, Phys. Rep. **565**, 1 (2015).

[26] H. E. Montgomery, K. D. Sen, and J. Katriel, Phys. Rev. A **97**, 022503 (2018).

[27] J. Katriel, H. E. Montgomery, and K. D. Sen, Phys. Plasmas **25**, 092111 (2018).

[28] A. S. Coolidge and H. M. James, Phys. Rev. **51**, 855 (1937).

[29] C. L. Pekeris, Phys. Rev. **112**, 1649 (1958).

[30] M. Bollhöfer and Y. Notay, Comput. Phys. Commun. **177**, 951 (2007).

[31] L. U. Ancarani and K. V. Rodriguez, Phys. Rev. A **89**, 012507 (2014).

[32] J. Garza, J.-M. Hernández-Pérez, J.-Z. Ramírez, and R. Vargas, J. Phys. B: At. Mol. Opt. Phys. **45**, 015002 (2012).

[33] A. L. Baskervielle, A. W. King, and H. Cox, R. Soc. Open Sci. **6**, 181357 (2019).

[34] C. Froese-Fischer, T. Brage, and P. Johnsson, *Computational Atomic Structure: An MCHF Approach* (Taylor & Francis, Philadelphia, 1997).

[35] T. Koga, Y. Kasai, and A. J. Thakkar, Int. J. Quantum Chem. **46**, 689 (1993).

[36] T. Koopmans, Phys. (Amsterdam, Neth.) **1**, 104 (1933).

[37] M. Reed and B. Simon, *Methods of Modern Mathematical Physics IV: Analysis of Operators* (Academic Press, New York, 1978).

[38] W. Thirring, *A Course in Mathematical Physics 3: Quantum Mechanics of Atoms and Molecules* (Springer, New York, 1981).

[39] X. R. Wang, Phys. Rev. A **46**, 7295 (1992).

[40] R. L. Hall, J. Phys. A **25**, 4459 (1992).

[41] R. L. Hall and Q. D. Katatbeh, J. Phys. A **35**, 8727 (2002).

[42] G. Chen, Phys. Rev. A **72**, 044102 (2005).

[43] R. L. Hall, Phys. Rev. Lett. **101**, 090401 (2008), and references therein.

[44] R. L. Hall and O. Yeşiltaş, J. Phys. A **43**, 195303 (2010).

[45] C. Semay, Phys. Rev. A **83**, 024101 (2011).

[46] R. L. Hall and P. Zorin, Ann. Phys. (Berlin) **527**, 408 (2015).

[47] J. L. Gázquez, A. Vela, and M. Galván, Phys. Rev. Lett. **56**, 2606 (1986).

[48] The NIST reference on constants, units, and uncertainty, https://physics.nist.gov/cuu/Constants/index.html.

[49] C. Aslangul, R. Constanciel, R. Daudel, and P. Kottis, Adv. Quantum Chem. **6**, 93 (1972).

[50] K. D. Sen, J. Chem. Phys. **123**, 074110 (2005).

[51] M. Rodriguez-Bautista, R. Vargas, N. Aquino, and J. Garza, Int. J. Quantum Chem. **118**, e25571 (2018).

[52] J.-H. Ou and Y. K. Ho, Atoms **7**, 70 (2019).

[53] M. A. Martínez-Sánchez, R. Vargas, and J. Garza, Quantum Rep. **1**, 208 (2019).

[54] C. E. Shannon, Bell Syst. Tech. J. **27**, 379 (1948).

[55] S. R. Gadre, S. B. Sears, S. J. Chakravorty, and R. D. Bendale, Phys. Rev. A **32**, 2602 (1985).